ACS APPLIED NANO MATERIALS

www.acsanm.org Article

Fluorographite Nanoplatelets with Covalent Grafting of Anion-Exchange Resins for Water Purification

Abhispa Sahu, Jeffrey R. Alston, Cliff Carlin, Matt Craps, Klinton Davis, Haley B. Harrison, Terawit Kongruengkit, Abhisek Manikonda, Sydney Elmore, Rachel Rollins, Bolaji Sadiku, Stephen Schmal, Juvairia Shajahan, and Jordan C. Poler*

Cite This: *ACS Appl. Nano Mater.* 2022, 5, 5709–5721 Read Online

ACCESS | Metrics & More | Article Recommendations | Supporting Information

ABSTRACT: We have developed a novel green synthetic method to covalently graft fluorographite (FGi) nanoplatelets, with quaternary ammonium polyelectrolyte chains under mild reaction conditions in water. Radical centers on the fluorographite layers react with the radical chain end on short strands of anion-exchange resins. While fluorographite is superhydrophobic, we show that the polymer radical chain end is necessary to initiate defluorination and delamination of the FGi in neutral pH water, without any pretreatment or caustic reagents. Scanning electron microscopy of thin films shows continuous and organized stacking of ellipsoidal nanoplatelets across large defect-free areas. We show that these new materials are highly effective at removing known and emerging contaminants to below environmentally relevant concentrations. Electron microscopy, vibrational spectroscopy, elemental analysis, and thermal analysis data are presented, and they are consistent with defluorination, partial exfoliation, and graphitization during the aqueous polymer grafting reaction. A radical-initiated mechanism is proposed that is consistent with the observed defluorination and oxidation of FGi nanoplatelets. The physicochemical properties, water flux, and morphology of these thin-film assemblies are described in detail. Thin membranes of polymer-functionalized fluorographite removed 99% of perfluorooctanoic acid to below 100 parts per trillion while maintaining a very high water flux over 1100 L h^{-1} m^{-2} bar^{-1}. Percent removal of perfluorinated alkyl substances and heavy metal oxyanions versus polyelectrolyte-functionalized fluorographite membrane areal density is reported. The methodology presented in this study is a facile approach toward developing high-performance materials for sustainable and green applications.

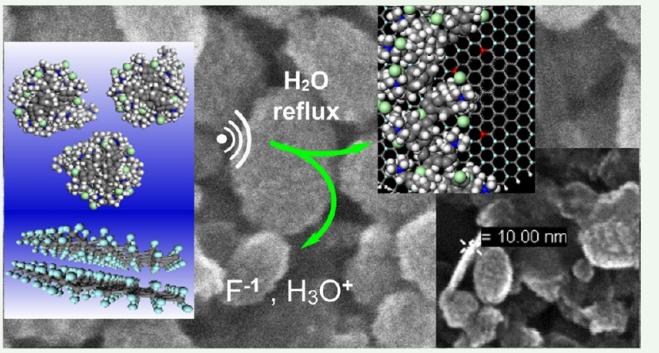

KEYWORDS: *fluorographite, graphite fluoride, nanoplatelets, aqueous defluorination, functionalization, polyelectrolyte, water purification*

1. INTRODUCTION

In this paper, we describe a green and facile synthesis of polymer-functionalized nanostructured carbon scaffolds. This aqueous process is efficient due to the radical-mediated reactivity of fluorographite (FGi). We show that FGi is a superior starting material, compared to graphite or graphene, for the synthesis of water purification membranes. Many graphite- or graphene-based materials have been studied for use in drinking water purification technologies. This is mostly due to their exceptional mechanical[1] and chemical stability, large specific surface area, and the ability to assemble them into nanoscale multilayer laminate thin films. Membrane purification technology requires the optimization of high water flux and efficient impurity removal. In general, graphene does not possess an intrinsic strong binding mechanism to water-soluble impurities. Moreover, most graphene-based membranes have very low water flux, typically <10 L m^{-2} h^{-1} bar^{-1}, and are thus not commercially viable. Even recent advances using chemically unzipped carbon nanotube membranes[2] have a limited water flux of up to 100 L m^{-2} h^{-1} bar^{-1}. To improve these properties, graphene dispersion and chemical modification have received significant study.[3,4] The modification and surface functionalization of graphite or graphene typically start with a chemically caustic process.[5,6] Most of these chemical methods require compounds that are harmful to human health and the environment. Consistent with the principles of green chemistry, material synthesis and processing should avoid caustic reagents and nonaqueous solvents. Fluorographite and fluorographene materials are widely used in various applications like corrosion-resistant coatings,[7] thermoelectric devices,[8]

Received: February 16, 2022
Accepted: March 21, 2022
Published: April 4, 2022

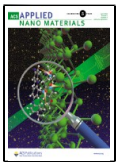

https://doi.org/10.1021/acsanm.2c00709
ACS Appl. Nano Mater. 2022, 5, 5709–5721

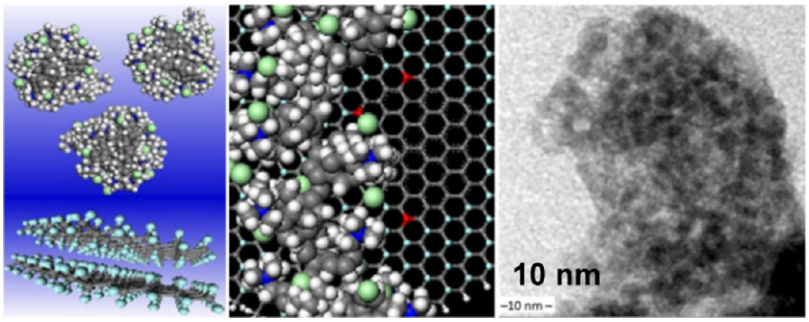

Figure 1. Molecular dynamics annealed poly(vbTMAC) and few-layered fluorographite are illustrated in the left panel, polymer and partially defluorinated graphene are shown in the center panel where the red atoms are radical centers, and TEM of polymer-functionalized fluorographite is shown in the right panel. Magnification 400,000×; scale bar 10 nm.

supercapacitors,[9] biosensing,[10] solar cells,[11] organic field-effect transistors,[12,13] and high-performance cathode materials.[14] All of these materials start with graphite or fluorographite and require nonaqueous synthetic methods or use solvents like *N*,*N*-dimethylformamide (DMF), *N*-methyl-2-pyrrolidone, or toluene to facilitate oxidation or exfoliation. Thus, alternative graphenic derivatives are required to allow cost-effective green processability and to achieve highly functionalized nanoscale materials that are capable of removing known and emerging contaminants to very low levels in water.

In this study, we demonstrate defluorination and partial exfoliation of fluorographite within an all-aqueous environment, utilizing the living radical chain end of short strands of polyelectrolytes at neutral pH. We have achieved defluorination to below 4 atom % using this green and sustainable method. Radical centers on fluorographite can interact with electron-rich or electron-donating species. Delocalization of spin centers due to the presence of C−F σ^* orbitals in the neighboring atoms can stabilize these singly occupied molecular orbitals (SOMOs).[15] These surface defects can act as the initiation sites of defluorination, which eventually increase upon reaction with electron-rich species. Although the C−F bonds have high chemical stability, due to the low-lying σ^* orbital of tertiary C−F bonds, they do react as electrophiles.[15,16] Studies have shown that defluorination of fluorographene follows an S_N2 nucleophilic substitution mechanism.[17] Additionally, the generation of spin centers/radical centers (fluorine vacancies) due to radical addition mechanisms from the solvent or the presence of electron-rich species has been shown to facilitate defluorination.[15,18,19] Otyepka et al. proposed that the defects in fluorographene contribute to its higher reactivity relative to other, more stable, perfluorocarbons. They postulated that point defects initiate a radical mechanism that drives defluorination in the presence of methyl radicals in an *N*,*N*-dimethylformamide environment.[15] Baumgartner et al. postulated that under aqueous conditions, the byproduct of defluorinated fluorobenzene is fluoride anions.[20] Kouloumpis et al. demonstrated defluorination of fluorographene under highly basic conditions (pH = 10−11), suggesting S_N2 nucleophilic substitution of the F atom by hydroxyl moieties.[19] Rajeena et al. performed a similar F substitution reaction in fluorographite using a 10 wt % ethanolic NaOH solution. Their process exfoliated fluorographite into hydroxy-substituted graphene.[21]

The defluorinated sites, created during our aqueous synthetic method, are potential centers for polyelectrolyte radical attack and subsequent covalent attachment. As the number of spin centers increases during the reaction, the resulting fluorographite becomes highly functionalized. It has previously been demonstrated that defluorination and subsequent delocalization of spin centers gave rise to a cascade of C=C bonds (or π-conjugated regions) in fluorographite.[15,18] We have observed a similar increase in sp^2-hybridized C with a commensurate loss of F from the solid material and an increase of fluoride ions in the reaction solution. The synthesis and characterization of these polyelectrolyte-functionalized fluorographite (PFG) resin materials are described below, and a potential mechanism is proposed. The illustration and transmission electron microscopic (TEM) image in Figure 1 are consistent with the data presented below.

The polymer-functionalized fluorographite materials in this study are particularly well suited for removing environmental contaminants of known and emerging concern. Removal of contaminants at very low concentration requires accessible binding sites with large binding equilibrium constants. Our PFG materials contain short polymer brushes of strong base anion (SBA)-exchange binding sites that are covalently functionalized to the layers within fluorographite nanoplatelets. Per- and polyfluoroalkyl substances (PFAS) have notoriously high thermal and chemical stability, making them resistant to environmental degradation. Therefore, these persistent and toxic impurities are pervasive throughout natural water systems. Recent studies have shown the presence of PFAS in human blood serum, breastmilk,[22] human urine,[23] and human embryonic fetal organs.[24] PFAS is an emerging threat to the environment and to human health. The PFG materials described here remove these contaminants from water to below their target concentration or their maximum concentration level (MCL) while maintaining high water flux through the purification membrane.

We have achieved ≥99% removal of all tested contaminants at environmentally relevant concentrations, and these PFG materials are easily regeneratable and readily reusable without any significant performance degradation. Hence, our green synthetic method provides an efficient platform for tailoring fluorographite-based materials with a high degree of functionalization.

2. EXPERIMENTAL SECTION

2.1. Chemicals and Materials. All reagents were used as purchased without additional purification or modification. Graphite, fluorinated, polymer (fluorographite, >61 wt % F) (Sigma-Aldrich, Lot #MKCJ1629) was used. Polymer synthesis and functionalization was based on (vinylbenzyl)trimethylammonium chloride (vbTMAC)

https://doi.org/10.1021/acsanm.2c00709
ACS Appl. Nano Mater. 2022, 5, 5709−5721

Scheme 1. Summary of Synthetic Methods[a]

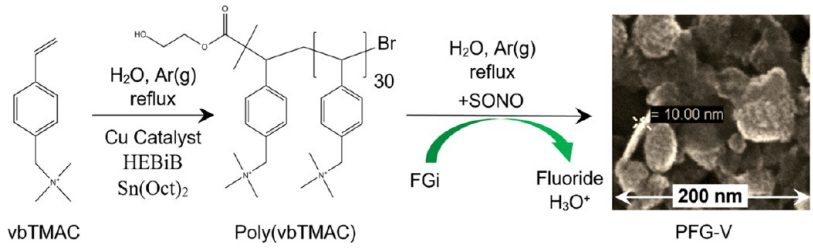

[a]Poly(vbTMAC) is grown using an aqueous ARGET-ATRP mechanism to >99% conversion with n = 30−35. Poly(vbTMAC) is mixed with pristine FGi powder and brought to reflux in water (see Section 2.3.2 and Table 1 for a summary of aqueous reaction conditions). During the synthesis of the polymer-functionalized fluorographite nanoplatelets, the reaction solution decreased in pH and increased in fluoride concentration as the PFG was defluorinated, partially exfoliated, and oxidized.

Table 1. Overview of Reagents/Processes for Various PFG Syntheses

reagents	PFG-I	PFG-II	PFG-III	PFG-IV	PFG-V	PFG-V+
TEMPO	+	−	−	−	−	−
catalyst/ligand complex	+	+	+	− (<5 ppm)	− (<5 ppm)	− (<0.1 ppm)
reducing agent	+	+	−	−	−	−
ultrasonication time (h)	2.3	2.3	2.3	0	2.3	26
reflux time (day)	3	3	3	3	3	3

(Fisher, 97%; Lot #A0311318) monomer, copper(II) bromide (Acros, 99+%; Lot #A0344238), tris(2-pyridylmethyl)amine (TPMA) (TCI, >98.0%; Lot #Z8GMO-AD) for the catalyst, stannous octoate ($Sn(Oct)_2$) (Sigma-Aldrich, 92.5−100%, Lot #SLBP5072V) for the reducing agent, and 2-hydroxyethyl 2-bromo-isobutyrate (HEBiB) (Sigma-Aldrich, 95%, Lot #MKBW2607) as the initiator. 2,2,6,6-Tetramethylpiperidine-1-oxyl (TEMPO) (Sigma-Aldrich, Lot #BCBZ3312) is the external radical. Other analytes include sodium chloride (Mallinckrodt Chemical, Lot #E42589) and disodium fluorescein (NaFL) (Sigma-Aldrich, Lot #BCBR1213V). Contaminants include perfluorooctanoic acid (PFOA) (Sigma-Aldrich, Lot #MKCC6736), potassium perfluorooctanesulfonate, 98% (PFOS) (Matrix Scientific, Lot #M22Q), and diatrizoic acid (DTZA) (Alfa Aesar, Lot #W24F030). Contaminants in the form of metalloid oxyanions of interest include potassium chromate (CrO_4^{2-}) (Alfa Aesar, Lot #9186184), sodium orthovanadate (VO_4^{3-}) (Alfa Aesar, Lot #Q21G501), ammonium tungstate (WO_4^{2-}) (Alfa Aesar, Lot #227051), and arsenic (V) oxide hydrate ($H_2AsO_4^{1-}$/$HAsO_4^{2-}$) (SPEX CertiPrep, Lot #25-72AS5M). Control studies included poly(ethylene glycol) methyl ether (Sigma-Aldrich, Lot #B2BR0088V).

2.2. Workup and Purification. Workup and purification of the synthesis required polypropylene membrane filters (0.45 μm pore size, 47 mm wide, Lot #2075-5), nitrocellulose mixed ester (MCE) (Advantec, Lot #70419200) with 0.2 μm pore diameter and 13 mm width and (Advantec, Lot #61202200) with 0.2 μm pore diameter and 25 mm width, 2 kDa MWCO dialysis membrane (Spectrum Labs, Lot #3294218) with 45 mm flat width and 29 mm diameter, 15 mL polypropylene centrifuge tubes (Corning, Lot #430052), and 50 kDa MWCO dialysis membrane (Spectrum Labs, Lot #3292110) with 34 mm flat width and 22 mm diameter. Membranes were activated by incubating for 10 min in deionized water under constant stirring. Microcon centrifugal filters (YM-100 Lot #R1CN67003) were used.

2.3. Synthetic Methods. The overall synthetic method is illustrated in Scheme 1. Poly(vbTMAC) is synthesized in water and then purified. FGi is added to the polymer solution in water and then functionalized with the living radical end of the stands.

2.3.1. Polymer Synthesis. The polyelectrolyte of vbTMAC was grown using the activator regeneration by electron-transfer assisting atom transfer radical polymerization (ARGET-ATRP) process as discussed in our previous publications to attain >95% conversion. In this case, the molar ratio between the monomer vbTMAC (1.60, 7.57 mmol) and the initiator HEBiB (31 μL, 214 μmol) was 35. Copper(II) bromide and tris(2-pyridylmethyl)amine (TPMA) were used to form the catalyst complex, and stannous octoate ($Sn(Oct)_2$) was used as the reducing agent for the ARGET-ATRP-mediated synthesis.[25,26] An aqueous solution of polyelectrolyte was purified of a reducing agent using the procedure similar to our previous publication.[25] The reaction mixture was centrifuged (200,000g, 60 min, 20 °C) for three iterations until there was no visible sedimentation of oxidized $Sn(OH)_2$(s) observed.

2.3.2. PFG-IV Synthesis and Purification. PFG-IV was synthesized in a two-step process: (1) 35-mers of poly(vbTMAC) was grown and purified, as discussed in Section 2.3.1. An aqueous solution of polyelectrolyte was purified of a reducing agent using the procedure similar to our previous publication.[25] The reaction mixture was centrifuged (200,000g, 60 min, 20 °C) for three iterations until there was no visible sedimentation of oxidized $Sn(OH)_2$(s) observed. (2) The purified polymer[25] solution was sparged with Ar(g) for 15 min and directly added to a Schlenk flask holding 15 mg of FGi. This mixture was shaken vigorously before sealing and heating to reflux in a 110 °C oil bath for 3 days under Ar(g)-positive pressure. As the reaction proceeded, the color of the reaction mixture changed to dark gray consistent with defluorination and graphitization of the FGi. After the required duration, functionalization was stopped by removing the heat. The reaction mixture was purified using the same steps as performed in our previous publications.[25] The dispersion was centrifuged (200,000g, 1 h, 20 °C) in high ionic strength (4 M NaCl(aq)) to mechanically disrupt any physisorbed polymer, and the sediments were collected. This process was repeated until the concentration of the unbound polymer in the supernatant was below the detection limit. This method did not use sonication, a catalyst, or a reducing agent during the FGi functionalization.

2.3.3. PFG-V Synthesis and Purification. PFG-V was synthesized using the purified polyelectrolyte described above. The polymer (16.6 mL) was sparged with Ar(g) for 15 min, and 9.0 mL was injected into a scintillation vial containing 15 mg of fluorographite. Because fluorographite is superhydrophobic, its dispersion in aqueous media is challenging. This mixture was ultrasonicated using a probe sonicator with the vial immersed in an ice water bath at 72 W cm^{-2} for 1 h and manually shaken once every 15 min. The hydrophobic fluorographite climbed up the walls of the vial until it became sufficiently coated with the polymer. After 1 h, the mixture was added back into the Schlenk flask, and the vial was rinsed with deionized water to transfer most of the fluorographite particles into the reaction mixture making a final volume of 22 mL. This dispersion was sparged for 10 min, sealed, and sonicated at 72 W cm^{-2} for 1 h 20 min. The sonication probe was

https://doi.org/10.1021/acsanm.2c00709
ACS Appl. Nano Mater. 2022, 5, 5709−5721

removed, the reaction mixture was sparged for 20 more minutes, sealed, and then heated to reflux in a 110 °C oil bath for 3 days under Ar(g)-positive pressure. As the reaction proceeded, the color of the reaction mixture changed to dark gray, which is a visual indicator of the defluorination process. After the required duration, functionalization was stopped by removing the heat. The reaction mixture was purified using the same steps as described in Section 2.3.2 and in our previous publications.[25,26]

2.3.4. PFG-V+ Synthesis and Purification. PFG-V+ was synthesized and purified under the same conditions as PFG-V except that the reaction was scaled up using 4.35 mL of polymer (0.500 g) and 157 mg of fluorographite into 200 mL of water into a Schlenk flask without temperature control. The solution was sparged with Ar(g) for 30 min and ultrasonicated under an Ar(g) blanket at 100 W cm^{-2} (500 W cm^{-2} at 1/5 duty cycle) for 26 h. This was followed by the standard 3 day reflux. An overview of the rest of the processes is given in Table 1, and the details are described in the Supporting Information.

2.4. Material Characterization. *2.4.1. Dynamic Light Scattering (DLS).* Hydrodynamic diameter and ζ-potential of various functionalized PFG batches were measured using the Malvern DLS Zetasizer instrument.

PFG sample solutions (10 ng mL^{-1}) were used for DLS measurements. For Zeta measurements, 2 mg L^{-1} of samples were used. An equilibrium time of 15 min was allowed in a normal room-temperature sample cell. All results were reported as value ± standard error, 95%, and outliers were removed.

2.4.2. Attenuated Total Reflectance Fourier Transform Infrared Spectroscopy (ATR FTIR). The ATR FTIR spectrometer (PerkinElmer, Spectrum 100) was used to observe the presence of a polymer within the PFG and compare it to control samples of fluorographite.

2.4.3. X-ray Photoelectron Spectroscopy (XPS). Samples were prepared by drop-casting PFG sample solutions on Si chips as a thin film. The XPS was an EscaLab 250Xi; a monochromatic (1487.6 eV) Al Kα-ray source was used to probe the surface, with a spot size of 250 μm, and a flood gun was used to limit charging at the surface of the materials. The Avantage Processing software package was used to analyze all XPS spectra.

2.4.4. X-ray Powder Diffraction. Crystal phases of PFGs were analyzed using X-ray powder diffraction (XRD) from PANalytical (Netherlands) X'Pert PRO. XRD patterns were measured over a 2θ range of 5−60 having a step size of 0.1000 with 10.0 s per step and a scan rate of 0.010° per step.

2.4.5. Transmission Electron Microscopy (TEM). The morphology of the ultrapurified samples was analyzed by transmission electron microscopy (JEOL JEM-2100Plus) at an acceleration voltage of 120 kV. For sample preparations, known concentrations of required dispersions were bath-sonicated for 5 min at 5 °C with occasional manual shaking. Prepared carbon mesh TEM grids were dipped into the dispersion and dried overnight. For electron energy loss spectroscopy (EELS) analysis, the emission current was set to 12 μA, the acquisition time was 1 s, the energy filter aperture was 30 μm, and the illumination angle was set to 1.250 mrad. Selected area diffraction (SAED) was measured of all of the samples deposited in TEM grids.

2.4.6. Scanning Electron Microscopy (SEM) and Energy-Dispersive X-ray (EDX) Spectroscopy. PFG thin films were made by dead-end filtration of dispersed particles onto an MCE support for SEM analysis only. An LEO 1550 column with a field emission gun, a 2 nm beam width, and a 30 μm aperture was used at 10 kV. SEM analysis was used for examining the morphology and edge thickness of PFG thin films. PFG thin films were drop-casted and dried on a Si chip for SEM/EDX analysis. The samples were examined using a JEOL JSM 6480 SEM operated by associated software. EDX analysis was used to compare the elemental composition of FGi with control specimens.

2.4.7. Thermogravimetric Analysis (TGA). Thermogravimetric analysis (Mettler SDTA851) of PFG and fluorographite samples was done in Air mode. Mettler software was used to analyze the measurements.

2.4.8. Water Flux Studies. For water flux measurements, thin films of PFG-V of different mass densities (0.09, 0.46 mg cm^{-2}) were used to evaluate the water flux using deionized water as permeate. A known mass of PFG was deposited on 25 mm wide 0.2 μm pore diameter MCE membranes as a thin film, and a known volume of deionized water was pushed through under vacuum with a known pressure. The duration for a known volume of deionized water to flow through was recorded, the exact pressure was recorded, and this process was repeated for several (>3) iterations. These thin films were dried for 30 min under vacuum, and the permeate flux was recorded again for several measurements. The water flux value was estimated from the following equation

$$J_w = \frac{Q}{AP\Delta t}$$

where J_w is the water flux (L m^{-2} h^{-1} bar^{-1}), Q is the volume of water (L), A is the surface area of the layers or film (m^2), P is the pressure (bar), and Δt is the time (h) required for volume L of deionized water to flow through.

2.4.9. Analyte Adsorption Studies. We tested the removal of compounds under the United States Environmental Protection Agency (U.S. EPA) emerging contaminant category to evaluate the potential of our materials as point-of-use water purification systems that can remove contaminants of immediate concern. We demonstrated the removal of perfluoroalkylated substances (PFAS) (viz., perfluorooctanoic acid (PFOA) and perfluorooctanesulfonate (PFOS)). Calibration standards (1−100 μg L^{-1}) and influent solutions for PFAS were prepared by serially diluting stock concentrations into deionized water. These stock concentrations (1−4 mg L^{-1}) were prepared by spiking distilled−deionized water with the analyte. Quantitative analysis of PFAS removal was by the electrospray mass spectrometry (MS, Thermo Scientific, LTQ Velos Pro) direct injection negative ion MS mode with mobile phase A comprising 0.5% formic acid in 100% LC-MS grade water and mobile phase B of 100% LC-MS grade acetonitrile. Quantitative analysis of all metal oxyanions (CrO_4^{2-}, VO_4^{3-}, WO_4^{2-} and arsenic (V) oxide hydrate ($H_2AsO_4^{1-}$/$HAsO_4^{2-}$)) was performed using inductively coupled plasma atomic emission spectroscopy (ICP OES, 5100 Agilent, California).

2.4.10. Regeneration Studies. A known mass of PFG-V was deposited onto a 25 mm wide 0.2 μm MCE membrane, and that membrane was placed in a glass vial. The film was allowed to incubate in a brine solution (1.5 mL, 2.0 M NaCl(aq)) for 5 min. The brine was disposed of, and deionized water was used to rinse the remaining brine (three replicates, 1.5 mL). A known volume and concentration of NaFL(aq) was added and allowed to incubate for 5 min, and the concentration of the NaFL(aq) solution after incubation was measured using UV−vis spectroscopy. In the subsequent cycles, the NaFL-saturated films were regenerated by incubating in successive brine solutions (1.5 mL, 2.0 M NaCl(aq)) until the concentration of the desorbed NaFL solution was reduced below 0.02 mg-C L^{-1} (the detection limit of NaFL using UV−vis). Brine rinses were followed by rinsing in deionized water to remove the salt. The cycle was repeated more than 30 times.

3. RESULTS AND DISCUSSION

3.1. Aqueous Synthesis of Poly(vbTMAC)-Functionalized Fluorographite (PFG). Fluorographite is an insulator with highly stable C−F bonds with bond dissociation energies larger than 418 kJ mol^{-1}.[17] However, many studies have demonstrated the instability of C−F bonds in fluorographite in the presence of nucleophiles and/or external radical agents. Yet, little research has been done in the field of covalent grafting of functional polymer brushes on defluorinated domains of fluorographite for sustainable applications.[27] In this study, we have investigated the surface modification and functionalization of fluorographite in the presence of polyelectrolyte brushes grown by a modified ARGET-ATRP

https://doi.org/10.1021/acsanm.2c00709
ACS Appl. Nano Mater. 2022, 5, 5709−5721

in water under neutral pH conditions (see Figure S12 for the reaction scheme).[25]

In Table 2, we summarize these defluorination results for a few of the materials characterized in this study. Specific synthetic details are described in Section 2.3 and in the Supporting Information. As purchased, pristine fluorographite contained 55 atom % F. The reaction of fluorographite with polyelectrolyte results in a significant decrease of F atom %. Many control experiments were also carried out to further specify the role of the polymer living radical chain end; these results are discussed below. When pristine fluorographite is refluxed in pure degassed water for 3 days, the material turns light gray but there is very little defluorination. When pristine fluorographite was stirred vigorously in degassed water at room temperature for 3 days, the material stays white and is not defluorinated, as expected (see Figures S10a,b and S11 in the Supporting Information). Sonicating pristine fluorographite in cold degassed water for 3−4 h does not change the properties of the hydrophobic material. The FGi stays white and remains stuck to the glass or sits on top of the water without dispersing into the water. To test the role of a polymer, poly(ethylene glycol) methyl ether (PEG) was mixed with pristine FGi. PEG is also a hydrophilic polymer with a similar molecular mass (PEG 5000 Da) as our polyelectrolyte (∼7500 Da). It was added at the same concentration as the poly(vbTMAC). After 3 days at reflux in degassed water, the PEG increased the dispersion of fluorographite. The physisorbed PEG acts as a surfactant around fluorographite particles. However, this PEG control did not result in significant FGi defluorination. Control experiments on pristine fluorographite in water with ARGET-ATRP reaction reagents (reducing agent or catalyst) both at cold temperature and at reflux did not result in any significant reduction of the F atom %, as detected by XPS or EDX. We conclude that low-temperature sonication alone, high-temperature reflux, the presence of ARGET-ATRP reaction reagents, or the addition of soluble polymers without living radical ends does not initiate the defluorination process, whereas the presence of the living radical chain end on the poly(vbTMAC) strand does result in partial exfoliation, dispersion, and defluorination of the fluorographite material.

Table 2. Elemental Composition (in Terms of Atom %) of Fluorographite, Fluorographite under Reflux (Control Studies), and PFG Resins Analyzed by XPS

element/material	carbon	fluorine	oxygen
pristine fluorographite	42.6	54.9	2.0
refluxed fluorographite (control)	42.7	55.3	2.0
PFG-I	34.8	20.3	43.9
PFG-IV	56.4	10.4	33.2
PFG-V+	63.0	3.6	33.4

All PFG samples are prepared by adding the poly(vbTMAC) polyelectrolyte into the aqueous reaction. These polymers are synthesized using an aqueous ARGET-ATRP method and are purified before the functionalization step. Each polymer strand P is terminated such that there is a living radical chain end, where $P - Br \leftrightharpoons P^{\bullet} + {}^{\bullet}Br$. It is this radical that initiates and propagates the functionalization of the FGi layers (Figure S12 for the reaction scheme). PFG-IV, PFG-V, and PFG-V+ are green aqueous processes that include only fluorographite and poly(vbTMAC) in water (residual catalyst < 5 ppm). After 3 days of reflux, without any sonication, PFG-IV defluorinated to F atom % = 10%. PFG-V+ was sonicated under Ar(g) for 26 h followed by reflux for 3 days. This resulted in an even lower F atom % = 3.6%. Future studies will measure the kinetics of defluorination and are not the subject of this study. XPS measurements on all of the PFG materials (PFG-I through PFG-V) show an increase in the O atom % due to the functionalization in water.

Fluorographite does not form stable dispersions in water, but after defluorination and functionalization in the presence of polyelectrolyte, it forms a stable black aqueous dispersion (Figure S1). Our observations are consistent with the reaction mechanism of fluorographite defluorination in the presence of TEMPO radicals, as discussed by Lai et al.[18] The incoming polyelectrolyte radicals can attack the fluorine atoms on fluorographite and generate spin centers. Spin centers are a good source of polyelectrolyte functionalization centers. An isolated spin center in a graphitic region is annotated as a red dot in Figure 1. Two spin centers adjacent to one another can result in the formation of C═C bonds. The generation of graphitic regions is detected in XPS analysis, where the deconvolution of the carbon peak of the PFG resin exhibits an intensified C═C bond peak. The radical living chain end $P^{\bullet}$ can attach to these tertiary carbon radicals on a fluorographite layer. Additionally, functionalization with styrenic polymers will also increase the percent of C═C bonds. Hence, thermogravimetric analysis (TGA) was performed to measure the degree of polymer functionalization discussed in Section 3.2.

3.2. Chemical Characterization of Poly(vbTMAC)-Functionalized Fluorographite (PFG). In this study, we have characterized the defluorination and functionalization of fluorographite mediated by ARGET-ATRP-assisted polyelectrolyte under several experimental conditions. The ATR FTIR spectra of purified PFG-IV resin confirmed the functionalization with polyelectrolyte strands (Figure 2, top). The IR band at 1638 cm^{-1} is characteristic of the C═C stretch of the styrene rings within the poly(vbTMAC). The PFG-IV C−H stretch at 2926 cm^{-1} (Figure 2, top inset) corresponds to the covalently attached poly(vbTMAC).[28] For comparison, the ATR FTIR spectra of pure poly(vbTMAC) are shown in Figure S2. This band at 2926 cm^{-1} is characteristic of the allyl C−H stretch on the vbTMAC after it has been polymerized (Figure 2, top inset). For the unreacted monomer, this C−H band appears at 3015 cm^{-1}. These films were rinsed extensively with brine and then with water to remove any residual polymer strands that were not covalently bound to the FGi. Pristine fluorographite exhibits a sharp IR absorption stretch at 1199 cm^{-1}, which corresponds to the C−F bond in the FGi. The intensity of the C−F stretching band in the IR spectra of PFG-IV was reduced and blue-shifted to 1207 cm^{-1} relative to the band in the IR spectra of the pristine FGi.[29]

The PFG materials have a large O atom % as determined by XPS. Below, we discuss the source of this oxidation during the aqueous reaction. Any −OH stretching at 3350 cm^{-1} is obscured by the broad absorption band characteristic of the poly(vbTMAC) (see Figure S2). Otyepka et al.[19] showed that heating FGi in the presence of aqueous hydroxide (pH 10−11) resulted in its partial defluorination (F atom % = 11%) and the covalent attachment of the −OH (O atom % = 26%) to a tertiary C on the FGi sheet by means of an S_N2 mechanism. The C−O stretch of a tertiary alcohol is in the range of 1200−1000 cm^{-1}. There is a small peak centered at 1050 cm^{-1} in the FTIR spectra of the PFG materials (Figure 2, bottom inset).

https://doi.org/10.1021/acsanm.2c00709
ACS Appl. Nano Mater. 2022, 5, 5709−5721

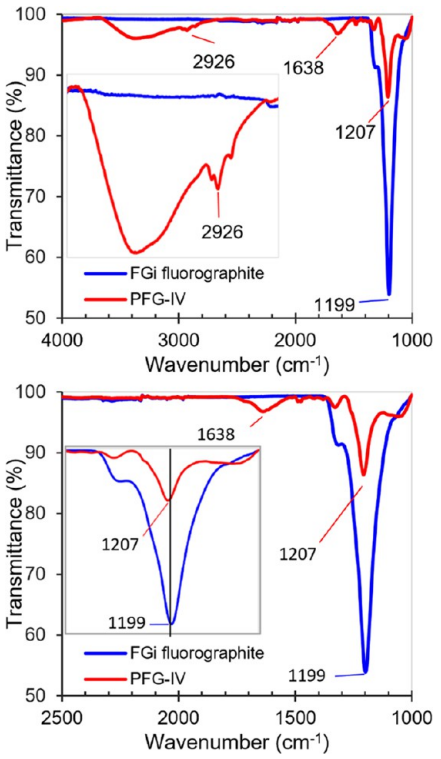

Figure 2. ATR FTIR spectra of fluorographite (blue) and PFG-IV (red), demonstrating defluorination and functionalization of poly(vbTMAC) on fluorographite. Top inset—characteristic poly(vbTMAC) band. Bottom and inset—characteristic C−F stretch in FGi.

This peak is convoluted with the C−F band of the FGi but is consistent with a tertiary −OH in the PFG.

Defluorination of PFG resins was confirmed by XPS analysis (Figure 3, top, and Table 2). Comparison of the C 1s spectra of fluorographite and PFG-IV shows (Figure 3, middle and bottom panels, respectively) a decrease in the intensity of the C−F bond peak at 288.4 eV for PFG. There is an increase of the peak at 284.6 eV due to the sp^2-hybridized carbon in the styrene group of the poly(vbTMAC) strands and possibly due to the graphitized regions of the defluorinated FGi. This analysis supports the case that we accomplished effective defluorination due to polymer attachment. This conclusion is also supported by EELS analysis. The F−K edge of fluorographite is compared with that of PFG-IV at 700 eV (Figure S3), where we observe a significant decrease in the intensity of the F signal in the PFG samples. The increase of the C−O peak at 286.5 eV is due to the defluorination process in water.

We observe a significant increase in the O atom % (from <2 to 33%) only when the fluorographite is reacted in the presence of the poly(vbTMAC) living radical chain end. The oxygen does not come from any of the functionalization reagents, and the reaction solution is sparged with Ar(g). There is only one O atom in the entire polymer strand, where the calculated O atom % in a 35-mer is 0.09% and is undetectable by XPS. There are no O atoms in the pristine FGi, and there are no oxidizing agents added to the aqueous reaction. It is possible that hydroxyl radicals from the sonication of some of the samples could attack the FGi; however, we see the same increase in O atom % within the PFG-IV sample that was not sonicated at all. Also, when we

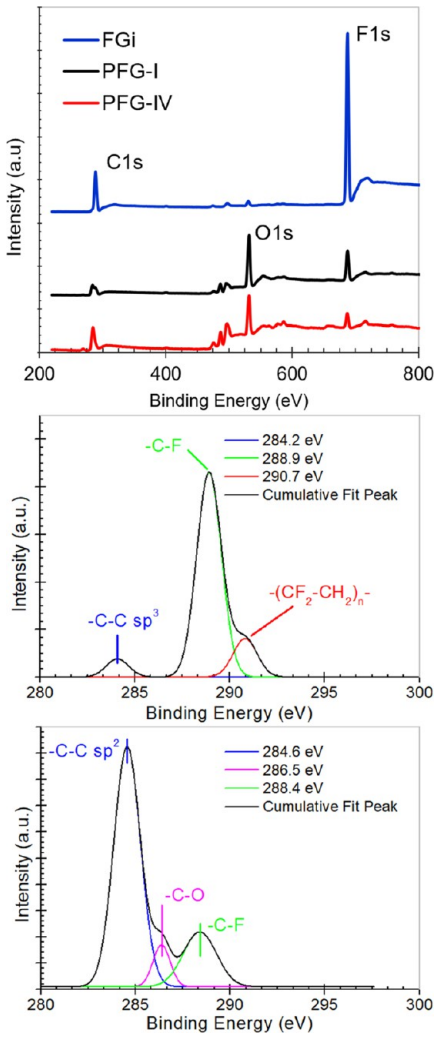

Figure 3. Survey scan of FGi, PFG-I, and PFG-IV (top). High-resolution C1 scan of FGi (middle) and PFG-IV (bottom). As functionalization increases, F atom % decreases and O atom % increases.

ultrasonicate pristine FGi in pure water held to <20 °C, the material stays white and hydrophobic and does not significantly defluorinate nor does the O atom % increase (XPS C atom % = 51%, F atom % = 48, and O atom % = 1.0%).

After 4 h of sonicating pristine FGi in water, a minimal amount of fluoride (2.2 ppm) was detected, and the solution maintained a pH = 5.5. The pH of air-saturated water is also 5.6. The reaction solution of the PFG-V+ synthesis was quite different. The PFG-V+ material was completely defluorinated and highly oxidized (XPS C atom % = 63%, F atom % = 3.6%, and O atom % = 33.4%). The fluoride concentration of the solution increased to 39 ppm. Most of the fluoride escapes from the reaction as HF(g). Interestingly, the pH of this reaction solution dropped to 1.5.

None of the reagents we add to the reaction lower the pH of the solution (i.e., poly(vbTMAC) in water, pH = 5.6, TPMA/$CuBr_2$ catalyst in water, pH = 5.6). Fluoride concentration and pH in the reaction solution during the reflux of FGi with poly(vbTMAC) were measured versus reflux time. The pH dropped continuously from 5.6 to 2.4 as the fluoride concentration in the solution increased from 2 to >30 ppm

https://doi.org/10.1021/acsanm.2c00709
ACS Appl. Nano Mater. 2022, 5, 5709−5721

after 132 h (Figure 4). As an additional control study, FGi was sonicated and then refluxed in Ar(g)-sparged water with only

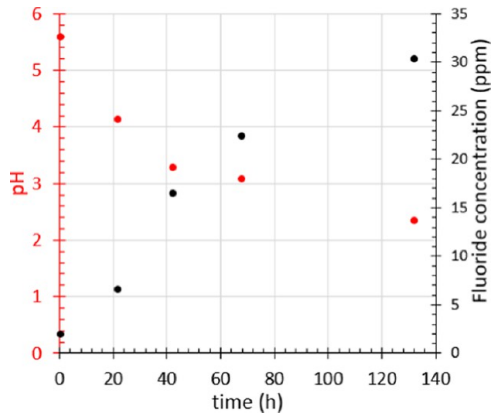

Figure 4. Reaction solution from refluxing PFG synthesis versus time. pH drops (red) as the fluoride concentration increases (black).

the monomer, vbTMAC, added. Aliquots pulled after 24 and 48 h resulted in no decrease in pH and a minimal increase of fluoride up to 5 ppm, while the FGi solids stayed white and hydrophobic.

A possible mechanism, which is consistent with our observations, is shown in Figure 5. Future studies will explore

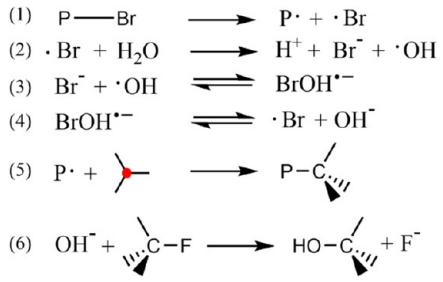

Figure 5. Proposed mechanism for defluorination and functionalization of FGi with poly(vbTMAC) living radical chains.

this mechanism in detail. When the polymer radical end, P—Br, attacks a radical vacancy (step 5, Figure 5) on the FGi sheet, a Br$^{\bullet}$ radical is liberated. This highly reactive species reacts with water to form hydrobromic acid, a strong acid, and $^{\bullet}$OH radicals (step 2, Figure 5). Bromide and the hydroxyl radical react to form the BrOH radical−anion (step 3, Figure 5) with a rate constant of 1.1×10^{10} M^{-1} s^{-1},[30,31] which decomposes to a bromine radical and hydroxide OH^- (step 4, Figure 5). It is known that at high temperature, the hydroxide can react with the C_3C−F sites of the fluorographite from the backside using an S_N2 mechanism,[19] liberating the fluoride (step 6, Figure 5) and leaving the acid in solution. This proposed mechanism is consistent with the drop in pH, the increase in fluoride in the solution during the reaction, and the increase in O atom % found by XPS of the PFG materials.

TGA was used to measure the thermal stability and mass degradation of purified PFG resins (Figures S13 and S4). Initially, all of the PFG samples show a 2−4% weight loss due to residual physisorbed water. Between 125 and 450 °C, the mass loss is from the decomposition of poly(vbTMAC) due to styrene and quaternary ammonium decomposition, where the trimethylammonium chloride decomposes to trimethylamine and HCl gas.[32] This is shown in Figure S4 (top), where pure poly(vbTMAC) is thermally decomposed in air. The second significant mass loss between 450 and 600 °C was due to the decomposition of the residual defluorinated FGi. These results are similar for all versions of the PFG material. Pristine FGi is thermally stable up to $t \sim 450$ °C. The high-temperature decomposition of FGi from 450 to 800 °C is shown in the TGA in Figure S4. These data are consistent with the literature,[33,34] where the pristine FGi material defluorinates and then oxidizes above 500 °C. The TGA of PFG-IV (Figure S13) is of a defluorinated material due to the polymer grafting reaction. During the polymer functionalization, the FGi loses F and the atom % of oxygen increases, consistent with the proposed mechanism in Figure 5. The purified PFG materials are over 50% by mass polymer. These data are consistent with polymer strands functionalized in between graphenic layers of the nanoplatelets described in Section 3.3.

3.3. Structural Characterization of Poly(vbTMAC) Functionalized Fluorographite (PFG). Transmission electron micrographs (TEMs) of fluorographite and PFG-IV are compared in Figure 6. These samples are highly purified by

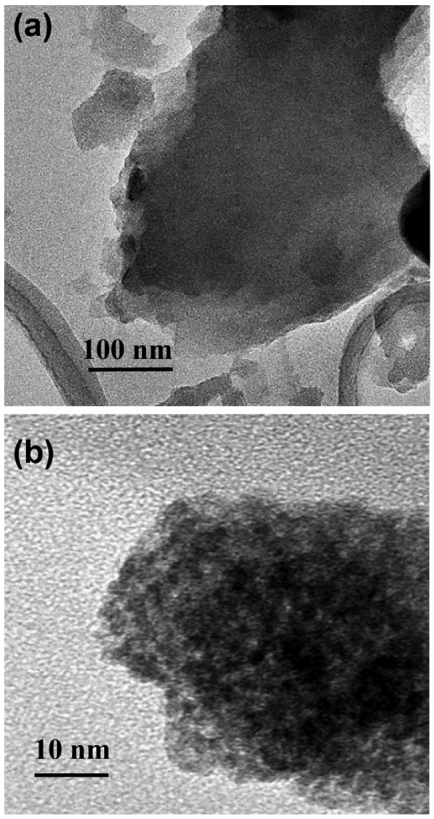

Figure 6. Transmission electron micrographs of few-layered fluorographite sheets (a) and purified PFG-IV (b). *d*-spacing calculations are shown in the Supporting Information. Magnification in (a) 50,000× and (b) 400,000×.

ultracentrifugation to remove all but the most dispersed nanoparticles. The larger nanoplatelets shown in the SEM images in Figure S5a are not present in the TEM samples. Fluorographite shows the stacking of layers of large sheets (Figure 6a), whereas the TEM of PFG exhibits a different morphology. At 400,000× magnification, the small PFG crystallites exhibit a platelet morphology with spheroidal particles. The dense globular functionalization is consistent

https://doi.org/10.1021/acsanm.2c00709
ACS Appl. Nano Mater. 2022, 5, 5709−5721

with poly(vbTMAC) brushes attached to the carbon nanoplatelet (Figure 6b). From our previous work,[25,26] we reported the radius of gyration of 26-mer units of polyelectrolyte to be 1.7 nm. The diameter of the globular structures at the surface of the few-layered fluorographite sheet is approximately 3 nm, suggesting that these are the polyelectrolyte brushes in highly functionalized domains. EELS analysis of these globular structures did not detect any N. The calculated N atom % is less than 1% and therefore close to the detection limit of the technique. SEM images (Figure S5a) also show globular/nodular polymer structures on the surface of the ellipsoidal nanoplatelet PFG crystallites.

XRD analysis of PFG-I was compared with pristine fluorographite. XRD of fluorographite (Figure 7, top panel)

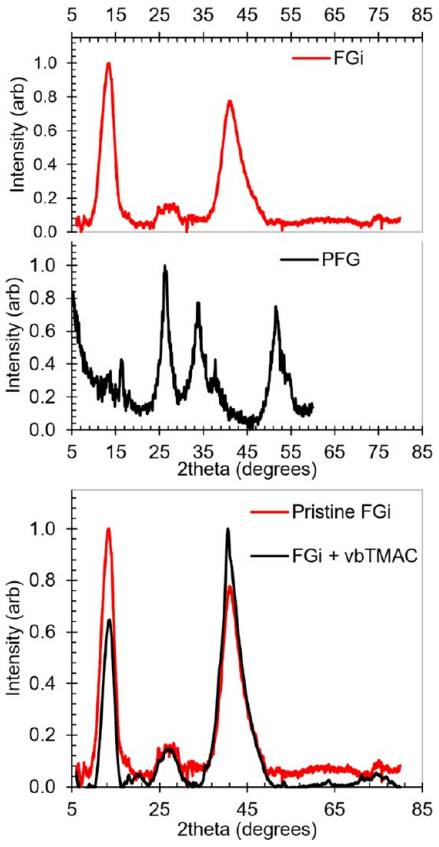

Figure 7. XRD patterns of pristine fluorographite (red, top) and PFG-I (black, top). XRD of pristine FGi is overlaid with an XRD of a control (bottom panel). This control shows that sonication, or reflux, or the presence of the monomer vbTMAC does not change the structure of the FGi.

shows a broadened (002) reflection peak at 2θ = 26.8° compared to the more intense and sharper peak at 2θ = 26.8° of the PFG-I sample. This is indicative of the resulting graphenic regions due to defluorination of the fluorographite after polymer functionalization.[35] This 2θ value corresponds to a *d*-spacing (or interlaminar spacing) of 0.33 nm (calculated from the Bragg relation shown in Table S1), which is consistent with the selected area electron diffraction (SAED) patterns of PFG-I and PFG-IV obtained by TEM analysis (Figure S7c,d and Table S1). Defluorination of the FGi due to radical-mediated polymer functionalization yields an increase in sp^2-hybridized graphenic layers. The (001) reflection peak at 2θ = 12.9° corresponds to the hexagonal structure with high fluorine content in the sp^3-hybridized fluorographite.[29] After polyelectrolyte functionalization (PFG-I), this 2θ = 12.9° peak was significantly reduced in the XRD and SAED analyses. Additionally, we observed that the diffusive rings of fluorographite SAED are in the transition phase of conversion to the highly ordered crystalline phase in PFG resins (Figure S7c,d).[36] The diffusive rings of fluorographite relating to reflection peaks of (001) and (100) are shown in Figure S7b–d.[21] As the atom % of F decreased during the different synthetic methods, the SAED reflections became sharper, which is consistent with an increase in graphitic regions throughout the nanoplatelets. This is consistent with our proposed mechanism and the model shown in Figure 1 (center), where C radicals can migrate along the graphenic planes and can be used to react with the living radical end of the poly(vbTMAC).

In the XRD of PFG-I, there is a shoulder near 2θ = 5°, which is too small of an angle to be fully resolved with our powder XRD. However, it is consistent with a much larger interlaminar spacing, where polymer strands are in between the graphenic layers. Song et al. showed this XRD peak to move steadily to smaller 2θ < 11° as the intercalating molecules increased in size.[37] Another characteristic reflection peak (004) was prominent at 2θ = 51.7°, which confirms the formation of the crystalline structure of graphite during defluorination.[38,39] This peak corresponds to a *d*-spacing of 0.18 nm, which is supported by SAED patterns of PFG-I and PFG-IV (Figure S7c,d and Table S1). A fluorographite diffraction peak at 2θ = 41.0° was visible in the SAED pattern of PFG-V corresponding to a *d*-spacing of 0.22 nm. This (100) reflection peak corresponds to the C−C in-plane length in the reticular system.[33,40,41] From XRD analysis, there is a reflection peak at 2θ = 33.9° for PFG-I, which corresponds to a d-spacing of 0.26 nm. This measurement agrees well with SAED patterns of PFG-I and PFG-IV (Figure S7c,d and Table S1).

XRD of control samples is compared in Figure 7, bottom panel. The control sample was made by mixing pristine FGi and excess vbTMAC monomer in water. The samples were sonicated for 2−3 h, and the FGi remained white and hydrophobic. The samples were then refluxed under Ar(g) for 3 days and then dried before XRD acquisition (Figure 7, lower (black line)). There were no structural changes to the fluorographite after sonication or reflux, nor under any aqueous conditions, so long as the radical chain end polymer was not present.

The hydrodynamic diameter and ζ-potential of PFGs were measured using the DLS Zetasizer (Figure S8). The measured hydrodynamic diameter of PFG-V was 76 ± 2.4 nm. These particle sizes are consistent with the size of the nanoplatelets measured from XRD and from SEM data.[42] The measured positive ζ-potential (+53.5 ± 0.46 mV) is consistent with a conformal coating of polyelectrolyte onto the fluorographite surface, as shown in Figure S9. These polyelectrolytes contain quaternary ammonium salts, giving the particles a significantly positive ζ-potential.

Morphology of the PFG resin thin-film assembly is an important parameter of the structure−property−function relationship. We performed SEM analysis on thin films of PFG-V+ to understand how the assembly of these functionalized particles contributes to effective contaminant removal while maintaining high water flux (Figure 8). A 700 nm thick PFG film (see Figure S5b for cross-sectional measurement) exhibited uniform horizontal stacking of nanoplatelets. The

https://doi.org/10.1021/acsanm.2c00709
ACS Appl. Nano Mater. 2022, 5, 5709−5721

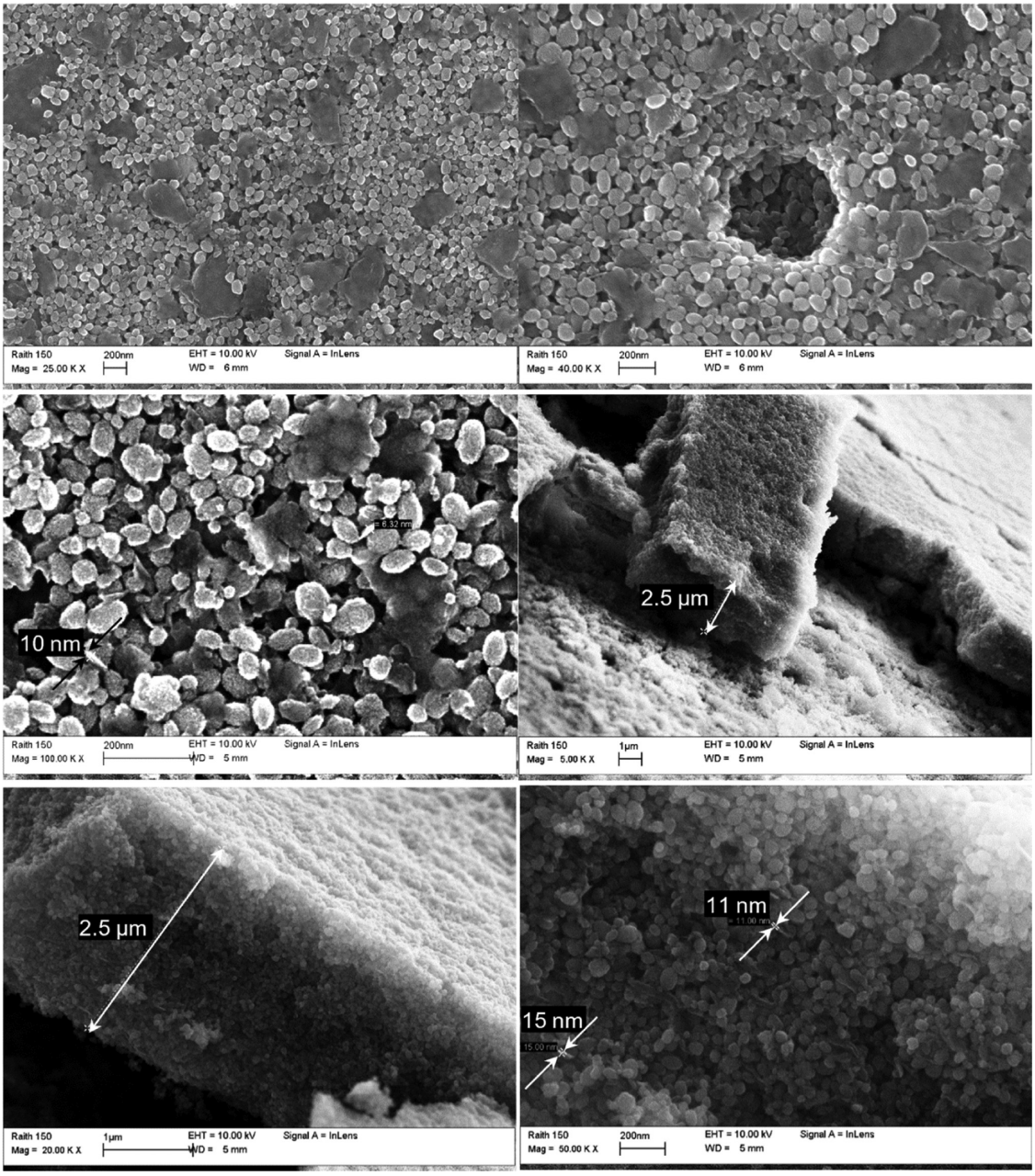

Figure 8. Scanning electron micrographs of the PFG-V+ thin film revealing a nanoplate-like morphology. Top left−right from a 700 nm thick film. Middle and bottom panels from a 2.5 μm thick film. The film was intentionally scratched to reveal membrane morphology throughout. Edge-on measurements of nanoplatelets are ∼10 nm thick.

film was uniform and smooth and did not contain pinholes or cracks (see Figure S5a for low- and higher-resolution images). In Figure 8b, we show an artifact due to dislodged impurity during processing. The artifact revealed a continuous stacking assembly of the crystallite layers, with the bottom layer having a similar horizontal assembly as the top one. Consistent with TEM analysis, the SEM image at 250,000× magnification also showed nanoplatelets conformally coated with polymer nodules (Figure S5a). The measured diameter of these nanoplatelets (∼70 nm) agrees with the number distribution of the measured hydrodynamic diameter of these crystallites using DLS.

A thicker 2.5 μm film is shown in Figure 8 (middle and bottom panels). Aligned nanoplatelets are shown from a top view in the left-middle panel and are similar to the thinner film. The film was intentionally scratched to reveal its cross section in Figure 8, right-middle and lower panels. The films appear uniform and void-free throughout.

These films are made from purified dispersions of PFG-V+. The dispersions were centrifuged, and the supernatant was passed through an MCE filter and then the membrane was washed with deionized water. As the sonication time during the synthesis increased, the particles became smaller and more homogeneous, as expected. The bottom four panels in Figure 8 show various images of a 2.5 μm thick film that was intentionally scratched to reveal the membrane's morphology throughout. The orientation of the nanoplatelets is not uniform. High-resolution images of edge-on particles show a typical nanoplatelet thickness of ∼10 nm. This is consistent with our XRD data. The number of layers in graphitic materials

https://doi.org/10.1021/acsanm.2c00709
ACS Appl. Nano Mater. 2022, 5, 5709−5721

can be calculated by combining the Debye−Scherrer ($D = \frac{K\lambda}{\beta \cos \theta}$) and Bragg equations ($d = \frac{\lambda}{2 \sin \theta}$) resulting in $N = (D/d + 1)$, where D is the average crystal height, d is the interplanar spacing, β is the full width at half-maxima, and λ is the wavelength of the X-ray source. D and d were calculated to be 4.52 and 0.34 nm, respectively, for the (002) reflection peak, which describes the interlayer spacing for PFG-I. With K equal to 0.89 for spherical crystals with cubic unit cells,[43] β as 1.887°, and λ as 0.154 nm, the calculated number of layers in the crystallites, N, is equal to 14.[44] The platelet thickness, as determined by SEM on-edge images, is ∼10 nm. The focused SEM beam width is 2−3 nm, so the measured thickness of the nanoplatelet is consistent with our model of graphitic regions separated by polymer-intercalated regions.

When the samples are not sonicated, they have a larger and more heterogeneous, grain-like morphology. In Figure S5c, we show SEM images of PFG-IV (top) and FGi (bottom) after refluxing in water (4 ppm ATRP Cu catalyst present). Neither sample was sonicated, but both samples were refluxed for 3 days in hot water. Figure S6 shows a TEM of the ellipsoidal particles of the same PFG-IV sample. PFG-IV material also included poly(vbTMAC) with a living radical chain end. Partial exfoliation, even without sonication, is observed. The platelets from the PFG-IV synthesis, without sonication, are 40−80 nm thick. The PFG-IV material is highly defluorinated and functionalized with polymers. Even without sonication, these materials effectively remove contaminants from water.

Water flux values of PFG-IV, shown in Table 3, are 10−50 times higher than typical water flux through graphene oxide membranes of similar thickness (at 1 atmospheric pressure).[45,46] The assembly and stacking of the PFG nanoplatelets facilitate molecular transport through a tortuous path while maintaining a high water flux. This tortuosity allows molecules to be in diffusive proximity to the exposed quaternary ammonium ions during molecular transport, which leads to fast "contact-like" adsorption. We observed a 3.3× decrease in water flux when the areal density (mg cm^{-2}) of the thin film was increased by 5 times, consistent with a uniform thin film without cracks or pinholes.

Table 3. Water Flux Measurements of PFG-V Thin Films Deposited on MCE Determined at Specific Pressure[a]

areal density (mg cm^{-2})	water flux (L h^{-1} m^{-2} bar^{-1})
0.094	3724 ± 519
0.469	1135 ± 9

[a]Multiple runs were measured and averaged.

3.4. Adsorption Capacity and Percent Removal of Emerging and Known Contaminants. For adsorption capacity studies, we prepared thin films of our materials onto a mixed ester cellulose (MCE) support. Spiked solutions were pushed through these membranes. The 3 mL of samples easily passed through the material. Even with a very short contact time, most of the analytes were effectively removed from the water. We tested PFOS and PFOA removal with a stock concentration of 95.64 and 95.02 μg L^{-1}, respectively, and achieved >99% removal using a PFG-V thin film (700 nm thick, 0.46 mg cm^{-2}) deposited on the MCE support. The effluent concentration was measured by EIS-MS (the method described in Section 2.4.9 and in the Supporting Information). Figure 9 shows the percent removal of several contaminants as a function of the PFG membrane density in mg PFG cm^{-2}. Our fast-filtration method removed the contaminants in a few seconds of film contact, while the very high water flux of 1135 L m^{-2} h^{-1} bar^{-1} was maintained at one atmosphere transmembrane pressure (Figure 9 and Table 3). The open resin microstructure of the PFG materials enables facile binding site accessibility. The method detection limit (MDL) of all of the contaminants screened using the MS method was below 1 μg L^{-1} (ppb).

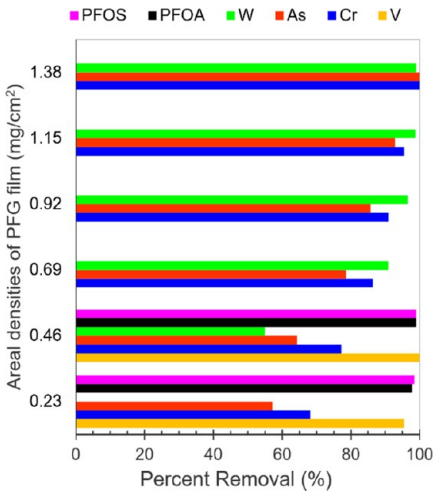

Figure 9. Percent removal of emerging contaminants by PFG-I and PFG-V+ (arsenate and tungstate removal) as a function of the areal density (mg cm^{-2}) of a PFG thin film deposited on the MCE membrane (13 mm wide, 0.2 μm pore size). Percent removal was measured using the fast-filtration method. Each colored bar represents a specific contaminant.

We measured the removal of metal oxyanions CrO_4^{2-}, VO_4^{3-}, WO_4^{2-}, and $H_2AsO_4^{1-}$/$HAsO_4^{2-}$ using PFG-V resins. MDL values in accordance with ICP OES and MCL values of these metal ions specified by U.S. EPA[47] are listed in Table S2. There is no MCL specified for W by U.S. EPA, but as a reference, we are considering the standard established by the Occupational Safety and Health Administration of 3 μg L^{-1} as a 15 min short-term exposure limit for airborne exposure to soluble tungsten.[48] Stock concentrations of these oxyanions were prepared above the MCL values but within the range of environmentally relevant concentrations, as shown in Table S2. We obtained a facile >99% removal of all oxyanions with effluent concentrations reaching well below their MCL (Figure 9).

Control studies were performed to analyze the sorption capacity of pristine fluorographite. Two milliliters of 3.00 mg-C L^{-1} of disodium fluorescein was incubated for 24 h with 1.0 mg of fluorographite, and the sample was filtered through a 13 mm wide 0.2 μm pore size MCE support. The remaining fluorescein in the effluent was measured using UV−vis spectroscopy. Less than 20% of the surrogate compound was removed due to nonspecific binding.

We measured the regeneration behavior of PFG-IV resins using a vial incubation protocol, as described in our previous works.[49] Figure 10 shows multiple adsorption−regeneration−reuse cycles of the PFG-IV materials. A membrane of PFG-IV was incubated in a surrogate contaminant (disodium fluorescein) until pseudoequilibration was reached. Then, the adsorptive loading q was measured by UV−vis of the solution. The film was then rinsed with brine to desorb the contaminant

https://doi.org/10.1021/acsanm.2c00709
ACS Appl. Nano Mater. 2022, 5, 5709−5721

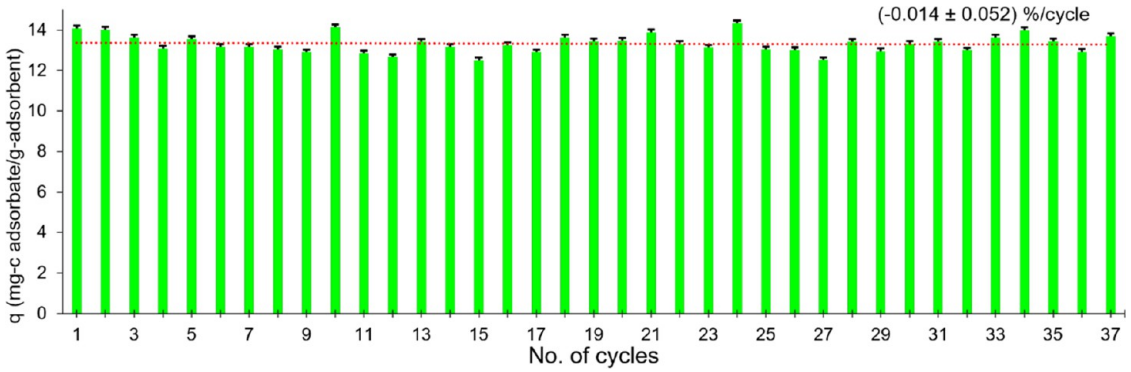

Figure 10. Regeneration and reusability studies of PFG-IV thin films using NaFL as a surrogate. A total of 37 cycles were repeated, which exhibited a 0.014% decrease in q per cycle.

and regenerate the material. The film was then rinsed with water to remove any salts and complete the cycle. Regeneration studies demonstrated a constant q of ∼13 mg-carbon of the fluorescein per gram of PFG resin. A slope of −0.014 ± 0.052% per cycle after 37 adsorption−desorption cycles is negligible and within experimental error. Without measurable loss of functionality, we project that these materials can be regenerated and reused for over 1000 cycles leading to a sustainable water purification solution.

4. CONCLUSIONS

In summary, this research was aimed at understanding and taking advantage of facile defluorination of and covalent grafting to fluorographite using green chemistry and processing. Aqueous defluorination and subsequent functionalization of fluorographite were performed to obtain functional nanomaterials for water purification purposes. These materials demonstrate a structure−property−function relationship, where high percent removal (>95%) capability is easily achieved while maintaining a high membrane water flux (1135 L m^{-2} h^{-1} bar^{-1}). Fast kinetics is achieved due to surface functionalization as compared to other porous or bead-like ion-exchange materials. PFGs demonstrated higher performance than graphene oxide analogues and other materials synthesized using caustic/toxic conditions.[2] TEM and SEM revealed crystalline nanoplatelets with poly-(vbTMAC)-functionalized domains. These resins were capable of high percent removal of emerging pervasive analytes under environmentally relevant concentrations to well below their MCL. These materials are also regeneratable and reusable without significant loss of performance. Therefore, highly functionalized PFG materials are compelling models for next-generation high-capacity removal of contaminants of emerging concern and other sustainable technology applications.

■ ASSOCIATED CONTENT

Supporting Information

The Supporting Information is available free of charge at https://pubs.acs.org/doi/10.1021/acsanm.2c00709.

Details of synthesis of all batches from PFG-I to PFG-V+; ATR FTIR of PFG-I; detailed method description of TGA and its analysis; scanning electron micrographs of thin-film assemblies of PFG-V and its edge thickness; TEM of PFG-V; SAED patterns of fluorographite and list of d-spacing values calculated by SAED pattern of PFGs; hydrodynamic diameter (nm) and ζ-potential (mV) measurements of PFG-V dispersion; summary of various concentrations of metalloid oxyanions for ICP OES; experimental description of control studies and their visual comparison; FTIR spectra; and pH and $[F^{-1}]$ measurements (PDF)

■ AUTHOR INFORMATION

Corresponding Author

Jordan C. Poler − *Department of Chemistry, University of North Carolina at Charlotte, Charlotte, North Carolina 28223, United States;* orcid.org/0000-0001-7691-4448; Phone: 704 687-8289; Email: jcpoler@uncc.edu

Authors

Abhispa Sahu − *Department of Chemistry, University of North Carolina at Charlotte, Charlotte, North Carolina 28223, United States;* orcid.org/0000-0002-3223-7577

Jeffrey R. Alston − *Joint School of Nanoscience and Nanoengineering, North Carolina A&T State University, Greensboro, North Carolina 27401, United States;* orcid.org/0000-0002-4177-0648

Cliff Carlin − *Department of Chemistry, University of North Carolina at Charlotte, Charlotte, North Carolina 28223, United States*

Matt Craps − *Joint School of Nanoscience and Nanoengineering, North Carolina A&T State University, Greensboro, North Carolina 27401, United States*

Klinton Davis − *Joint School of Nanoscience and Nanoengineering, North Carolina A&T State University, Greensboro, North Carolina 27401, United States*

Haley B. Harrison − *Joint School of Nanoscience and Nanoengineering, North Carolina A&T State University, Greensboro, North Carolina 27401, United States*

Terawit Kongruengkit − *Department of Chemistry, University of North Carolina at Charlotte, Charlotte, North Carolina 28223, United States*

Abhisek Manikonda − *Infrastructure and Environmental Systems, University of North Carolina, Charlotte, North Carolina 28223, United States;* orcid.org/0000-0001-9011-4754

Sydney Elmore − *Department of Chemistry, University of North Carolina at Charlotte, Charlotte, North Carolina 28223, United States*

Rachel Rollins − *Department of Chemistry, University of North Carolina at Charlotte, Charlotte, North Carolina 28223, United States*

https://doi.org/10.1021/acsanm.2c00709
ACS Appl. Nano Mater. 2022, 5, 5709−5721

Bolaji Sadiku − *Joint School of Nanoscience and Nanoengineering, North Carolina A&T State University, Greensboro, North Carolina 27401, United States*
Stephen Schmal − *Department of Chemistry, University of North Carolina at Charlotte, Charlotte, North Carolina 28223, United States;* orcid.org/0000-0001-9880-6448
Juvairia Shajahan − *Joint School of Nanoscience and Nanoengineering, North Carolina A&T State University, Greensboro, North Carolina 27401, United States;* orcid.org/0000-0001-6389-1910

Complete contact information is available at: https://pubs.acs.org/10.1021/acsanm.2c00709

Author Contributions

A.S.: conceptualization, methodology, validation, formal analysis, investigation, data curation, writing—original draft, writing—review and editing, visualization, supervision, and funding acquisition; J.R.A. and C.C.: investigation, data curation, visualization, and supervision; M.C., K.D., H.B.H., and S.S.: investigation, data curation, and visualization; T.K., R.R., B.S., S.E., and J.S.: investigation. A.M.: investigation and data curation; J.C.P.: conceptualization, methodology, validation, formal analysis, investigation, data curation, writing—original draft, writing—review and editing, visualization, supervision, project administration, and funding acquisition.

Notes

The authors declare no competing financial interest.

■ ACKNOWLEDGMENTS

The research work of A.S. was supported by the Graduate School Summer Fellowship Program (2019), the Graduate Assistant Support Plan (2016-21), and the Nanoscale Science Program at the University of North Carolina at Charlotte. This material was based upon work supported by the National Science Foundation under Grant No. 1450417. The authors thank Dr. Juan Vivero-Escoto for use of his DLS and ζ-potential instrumentation.

■ REFERENCES

(1) Nine, M. J.; Cole, M. A.; Tran, D. N. H.; Losic, D. Graphene: a multipurpose material for protective coatings. *J. Mater. Chem. A* **2015**, *3*, 12580−12602. Review.
(2) Han, Z.; Xiao, X.; Qu, H.; Hu, M.; Au, C.; Nashalian, A.; Xiao, X.; Wang, Y.; Yang, L.; Jia, F.; et al. Ultrafast and Selective Nanofiltration Enabled by Graphene Oxide Membranes with Unzipped Carbon Nanotube Networks. *ACS Appl. Mater. Interfaces* **2022**, *14*, 1850−1860.
(3) Yu, W.; Sisi, L.; Haiyan, Y.; Jie, L. Progress in the functional modification of graphene/graphene oxide: a review. *RSC Adv.* **2020**, *10*, 15328−15345.
(4) Johnson, D. W.; Dobson, B. P.; Coleman, K. S. A manufacturing perspective on graphene dispersions. *Curr. Opin. Colloid Interface Sci.* **2015**, *20*, 367−382.
(5) Hummers, W. S.; Offeman, R. E. Preparation of graphitic oxide. *J. Am. Chem. Soc.* **1958**, *80*, 1339. Article.
(6) Furst, A.; Berlo, R. C.; Hooton, S. Hydrazine as a reducing agent for organic compounds (catalytic hydrazine reductions. *Chem. Rev.* **1965**, *65*, 51−68.
(7) Yang, Z. Q.; Sun, W.; Wang, L. D.; Li, S. J.; Zhu, T. Z.; Liu, G. C. Liquid-phase exfoliated fluorographene as a two dimensional coating filler for enhanced corrosion protection performance. *Corros. Sci.* **2016**, *103*, 312−318.
(8) Huang, W. X.; Pei, Q. X.; Liu, Z. S.; Zhang, Y. W. Thermal conductivity of fluorinated graphene: A non-equilibrium molecular dynamics study. *Chem. Phys. Lett.* **2012**, *552*, 97−101. Article.
(9) Bulusheva, L. G.; Tur, V. A.; Fedorovskaya, E. O.; Asanov, I. P.; Pontiroli, D.; Ricco, M.; Okotrub, A. V. Structure and supercapacitor performance of graphene materials obtained from brominated and fluorinated graphites. *Carbon* **2014**, *78*, 137−146.
(10) Urbanová, V.; Karlicky, F.; Matej, A.; Sembera, F.; Janousek, Z.; Perman, J. A.; Ranc, V.; Cepe, K.; Michl, J.; Otyepka, M.; et al. Fluorinated graphenes as advanced biosensors - effect of fluorine coverage on electron transfer properties and adsorption of biomolecules. *Nanoscale* **2016**, *8*, 12134−12142.
(11) Das, S.; Sudhagar, P.; Verma, V.; Song, D.; Ito, E.; Lee, S. Y.; Kang, Y. S.; Choi, W. Amplifying Charge-Transfer Characteristics of Graphene for Triiodide Reduction in Dye-Sensitized Solar Cells. *Adv. Funct. Mater.* **2011**, *21*, 3729−3736.
(12) Zhu, M. S.; Xie, X. D.; Guo, Y. L.; Chen, P. L.; Ou, X. W.; Yu, G.; Liu, M. H. Fluorographene nanosheets with broad solvent dispersibility and their applications as a modified layer in organic field-effect transistors. *Phys. Chem. Chem. Phys.* **2013**, *15*, 20992−21000.
(13) Ho, K. I.; Huang, C. H.; Liao, J. H.; Zhang, W. J.; Li, L. J.; Lai, C. S.; Su, C. Y. Fluorinated Graphene as High Performance Dielectric Materials and the Applications for Graphene Nanoelectronics. *Sci. Rep.* **2014**, *4*, No. 5893.
(14) Li, Y.; Jian, Z.; Lang, M.; Zhang, C.; Huang, X. Covalently Functionalized Graphene by Radical Polymers for Graphene-Based High-Performance Cathode Materials. *ACS Appl. Mater. Interfaces* **2016**, *8*, 17352−17359.
(15) Medve', M.; Zoppellaro, G.; Ugolotti, J.; Matochova, D.; Lazar, P.; Pospisil, T.; Bakandritsos, A.; Tucek, J.; Zboril, R.; Otyepka, M. Reactivity of fluorographene is triggered by point defects: beyond the perfect 2D world. *Nanoscale* **2018**, *10*, 4696−4707. Article.
(16) Sandford, G. Perfluoroalkanes. *Tetrahedron* **2003**, *59*, 437−454. Review.
(17) Dubecký, M.; Otyepkova, E.; Lazar, P.; Karlicky, F.; Petr, M.; Cepe, K.; Banas, P.; Zboril, R.; Otyepka, M. Reactivity of Fluorographene: A Facile Way toward Graphene Derivatives. *J. Phys. Chem. Lett.* **2015**, *6*, 1430−1434. Article.
(18) Lai, W. C.; Xu, D. Z.; Wang, X.; Wang, Z. M.; Liu, Y.; Zhang, X. J.; Li, Y. L.; Liu, X. Y. Defluorination and covalent grafting of fluorinated graphene with TEMPO in a radical mechanism. *Phys. Chem. Chem. Phys.* **2017**, *19*, 24076−24081.
(19) Kouloumpis, A.; Chronopoulos, D. D.; Potsi, G.; Pykal, M.; Vlcek, J.; Scheibe, M.; Otyepka, M. One-Step Synthesis of Janus Fluorographene Derivatives. *Chem. - Eur. J.* **2020**, *26*, 6518−6524.
(20) Baumgartner, R.; McNeill, K. Hydrodefluorination and hydrogenation of fluorobenzene under mild aqueous conditions. *Environ. Sci. Technol.* **2012**, *46*, 10199−10205.
(21) Rajeena, U.; Akbar, M.; Raveendran, P.; Ramakrishnan, R. M. Fluorographite to hydroxy graphene to graphene: a simple wet chemical approach for good quality graphene. *New J. Chem.* **2018**, *42*, 9658−9665. Article.
(22) Ssebugere, P.; Sillanpää, M.; Matovu, H.; Wang, Z.; Schramm, K.-W.; Omwoma, S.; Wanasolo, W.; Ngeno, E. C.; Odongo, S. Environmental levels and human body burdens of per-and poly-fluoroalkyl substances in Africa: A critical review. *Sci. Total Environ.* **2020**, *739*, No. 139913.
(23) Wu, N.; Cai, D.; Guo, M.; Li, M.; Li, X. Per-and polyfluorinated compounds in saleswomen's urine linked to indoor dust in clothing shops. *Sci. Total Environ.* **2019**, *667*, 594−600.
(24) Mamsen, L. S.; Björvang, R. D.; Mucs, D.; Vinnars, M.-T.; Papadogiannakis, N.; Lindh, C. H.; Andersen, C. Y.; Damdimopoulou, P. Concentrations of perfluoroalkyl substances (PFASs) in human embryonic and fetal organs from first, second, and third trimester pregnancies. *Environ. Int.* **2019**, *124*, 482−492.
(25) Sahu, A.; Sheikh, R.; Poler, J. C. Green sonochemical synthesis, kinetics and functionalization of nanoscale anion exchange resins and

their performance as water purification membranes. *Ultrason. Sonochem.* **2020**, *67*, No. 105163.
(26) Sahu, A.; Blackburn, K.; Qumhiyeh, M. H.; Durkin, K.; Poler, J. In *Novel Nanomaterials for Water Purification: Synthesis, Characterization and Application of Functionalized SWCNTs*, Abstracts of Papers, 255th ACS National Meeting & Exposition, New Orleans, LA, United States; American Chemical Society, March 18–22, 2018; pp COLL–621.
(27) Feng, C.; Huang, X. Polymer Brushes: Efficient Synthesis and Applications. *Acc. Chem. Res.* **2018**, *51*, 2314–2323.
(28) Johnson, B. R.; Eldred, T. B.; Nguyen, A. T.; Payne, W. M.; Schmidt, E. E.; Alansari, A. Y.; Amburgey, J. E.; Poler, J. C. High-Capacity and Rapid Removal of Refractory NOM Using Nanoscale Anion Exchange Resin. *ACS Appl. Mater. Interfaces* **2016**, *8*, 18540–18549. Article.
(29) Yang, Y.; Lu, G. L.; Li, Y. J.; Liu, Z. Z.; Huang, X. Y. One-Step Preparation of Fluorographene: A Highly Efficient, Low-Cost, and Large-Scale Approach of Exfoliating Fluorographite. *ACS Appl. Mater. Interfaces* **2013**, *5*, 13478–13483. Article.
(30) Matthew, B. M.; George, I.; Anastasio, C. Hydroperoxyl radical ($HO_2^{\bullet}$) oxidizes dibromide radical anion ($^{\bullet}Br_2^-$) to bromine (Br_2) in aqueous solution: Implications for the formation of Br_2 in the marine boundary layer. *Geophys. Res. Lett.* 2003, *30* (24), 2297.
(31) Lei, Y.; Lei, X.; Yu, Y.; Li, K.; Li, Z.; Cheng, S.; Ouyang, G.; Yang, X. Rate Constants and Mechanisms for Reactions of Bromine Radicals with Trace Organic Contaminants. *Environ. Sci. Technol.* **2021**, *55*, 10502–10513.
(32) Ianchis, R.; Donescu, D.; Cinteza, L. O.; Purcar, V.; Nistor, C. L.; Petcu, C.; Nicolae, C. A.; Gabor, R.; Preda, S. Polymer-clay nanocomposites obtained by solution polymerization of vinyl benzyl triammonium chloride in the presence of advanced functionalized clay. *J. Chem. Sci.* **2014**, *126*, 609–616. Article.
(33) Gong, P. W.; Wang, Z. F.; Wang, J. Q.; Wang, H. G.; Li, Z. P.; Fan, Z. J.; Xu, Y.; Han, X. X.; Yang, S. R. One-pot sonochemical preparation of fluorographene and selective tuning of its fluorine coverage. *J. Mater. Chem.* **2012**, *22*, 16950–16956. Article.
(34) Sun, C. B.; Feng, Y. Y.; Li, Y.; Qin, C. Q.; Zhang, Q. Q.; Feng, W. Solvothermally exfoliated fluorographene for high-performance lithium primary batteries. *Nanoscale* **2014**, *6*, 2634–2641. Article.
(35) Ramoraswi, N. O.; Ndungu, P. G. Photo-Catalytic Properties of TiO2 Supported on MWCNTs, SBA-15 and Silica-Coated MWCNTs Nanocomposites. *Nanoscale Res. Lett.* **2015**, *10*, No. 427. Article.
(36) Rajeena, U.; Raveendran, P.; Ramakrishnan, R. M. Stepwise defluorination of fluorographene: How do the structural features govern the rates of heterogeneous electron transfer? *J. Fluorine Chem.* **2020**, *235*, No. 109555.
(37) Song, B.; Zhao, J. X.; Wang, M. J.; Mullavey, J.; Zhu, Y. T.; Geng, Z. S.; Chen, D. C.; Ding, Y.; Moon, K. S.; Liu, M. L.; et al. Systematic study on structural and electronic properties of diamine/triamine functionalized graphene networks for supercapacitor application. *Nano Energy* **2017**, *31*, 183–193.
(38) Ban, F. Y.; Majid, S. R.; Huang, N. M.; Lim, H. N. Graphene Oxide and Its Electrochemical Performance. *Int. J. Electrochem. Sci.* **2012**, *7*, 4345–4351.
(39) Sayah, A.; Habelhames, F.; Bahloul, A.; Nessark, B.; Bonnassieux, Y.; Tendelier, D.; El Jouad, M. Electrochemical synthesis of polyaniline-exfoliated graphene composite films and their capacitance properties. *J. Electroanal. Chem.* **2018**, *818*, 26–34.
(40) Ye, X. Y.; Gong, P. W.; Wang, J. Q.; Wang, H. G.; Ren, S. L.; Yang, S. R. Fluorinated graphene reinforced polyimide films with the improved thermal and mechanical properties. *Composites, Part A* **2015**, *75*, 96–103. Article.
(41) Tian, R.; Jia, X. H.; Yang, J.; Li, Y.; Song, H. J. Large-scale, green, and high-efficiency exfoliation and noncovalent functionalization of fluorinated graphene by ionic liquid crystal. *Chem. Eng. J.* **2020**, *395*, No. 125104. Article.
(42) Lotya, M.; Rakovich, A.; Donegan, J. F.; Coleman, J. N. Measuring the lateral size of liquid-exfoliated nanosheets with dynamic light scattering. *Nanotechnology* **2013**, *24*, No. 265703. Article.
(43) Sharma, R.; Chadha, N.; Saini, P. Determination of defect density, crystallite size and number of graphene layers in graphene analogues using X-ray diffraction and Raman spectroscopy. *Indian J. Pure Appl. Phys.* **2017**, *55*, 625–629. Article.
(44) Stobinski, L.; Lesiak, B.; Malolepszy, A.; Mazurkiewicz, M.; Mierzwa, B.; Zemek, J.; Jiricek, P.; Bieloshapka, I. Graphene oxide and reduced graphene oxide studied by the XRD, TEM and electron spectroscopy methods. *J. Electron Spectrosc. Relat. Phenom.* **2014**, *195*, 145–154. Article.
(45) Lian, B.; Deng, J.; Leslie, G.; Bustamante, H.; Sahajwalla, V.; Nishina, Y.; Joshi, R. K. Surfactant modified graphene oxide laminates for filtration. *Carbon* **2017**, *116*, 240–245.
(46) You, Y.; Jin, X. H.; Wen, X. Y.; Sahajwalla, V.; Chen, V.; Bustamante, H.; Joshi, R. K. Application of graphene oxide membranes for removal of natural organic matter from water. *Carbon* **2018**, *129*, 415–419.
(47) *2018 Edition of the Drinking Water Standards and Health Advisories Tables*; USEPA, 2018. https://www.epa.gov/sites/production/files/2018-03/documents/dwtable 2018.pdf.
(48) *Technical Fact Sheet – Tungsten*; USEPA, 2014. https://www.epa.gov/sites/production/files/2014-03/documents/ffrrofact-sheet_contaminant_tungsten_january2014_final.pdf.
(49) Sahu, A.; Blackburn, K.; Durkin, K.; Eldred, T. B.; Johnson, B. R.; Sheikh, R.; Amburgey, J. E.; Poler, J. C. Green synthesis of nanoscale anion exchange resin for sustainable water purification. *Environ. Sci.: Water Res. Technol.* **2018**, *4*, 1685–1694.

https://doi.org/10.1021/acsanm.2c00709
ACS Appl. Nano Mater. 2022, 5, 5709–5721